Electric Field Fluctuations Drive Vibrational Dephasing in Water

ARTICLE *in* THE JOURNAL OF PHYSICAL CHEMISTRY A · NOVEMBER 2005

Impact Factor: 2.69 · DOI: 10.1021/jp051364m · Source: PubMed

3 AUTHORS, INCLUDING:

Andrei Tokmakoff
University of Chicago
153 PUBLICATIONS **8,075** CITATIONS

SEE PROFILE

Electric Field Fluctuations Drive Vibrational Dephasing in Water

Joel D. Eaves and Andrei Tokmakoff*

Department of Chemistry and George Harrison Spectroscopy Laboratory, Massachusetts Institute of Technology, Cambridge, Massachusetts 02139

Phillip L. Geissler

Department of Chemistry, University of California and Physical Biosciences Division and Materials Sciences Division, Lawrence Berkeley National Laboratory, Berkeley, California 94720

Received: March 15, 2005; In Final Form: June 17, 2005

We present a microscopic description of the vibrational spectroscopy of the OH stretch of HOD in liquid D_2O. Our model predicts that OH frequency correlations decay with a sharp and rapid (≈35 fs) decrease, followed by a beat at ≈125 fs from intermolecular oxygen vibrations. On a short time scale (≈200 fs), ultrafast infrared spectroscopy of the OH stretch is sensitive to localized intermolecular motions. For times longer than ≈200 fs, cooperative molecular rearrangements drive dephasing. The interplay of electric field fluctuations, both local and cooperative, dictate vibrational frequency shifts and destroy vibrational coherence in water.

I. Introduction

Hydrogen bonds are the scaffolding of life, bridging adjacent strands of nucleic acids, stiffening proteins, and functionalizing enzymes. Liquid water forms a network of hydrogen bonds that connects molecular participants together. By simulating empirical models of water, researchers have made substantial progress in identifying the molecular motions and fluctuations that generate fleeting fractures in the network and entice molecules to "change allegiances" by trading hydrogen bonding partners.[1−4] Unfortunately, experiments by themselves have been relatively unfruitful in revealing truly microscopic motions in water. Thermal averaging in linear spectroscopies and scattering experiments makes it impossible to detect signatures from groups of molecules in subtly different environments.[5−8] However, provided there is a well-defined relationship between the vibrational transition frequency and the structure of the molecular liquid, nonlinear-IR spectroscopy overcomes this obstacle by coherently preparing molecules in spectrally distinct environments and measuring their subsequent relaxation dynamics.[9] From this perspective, the frequency becomes a marker through which one can monitor the dynamics of the liquid as it moves through its myriad of possible configurations.

The coordinates that are often used to identify a hydrogen bond between two water molecules depend only on the relative distance and orientations of two molecules (see ref 3, for example). On the length scales of these connections (≈3 Å), one imagines that the availability of nearby hydrogen bonds dictates the structure and dynamics of the liquid, but a hydrogen bonded pair also interacts with more distant partners through a network of hydrogen bonds. The fluctuations of the network can entice the hydrogen bonded pair to sever its hydrogen bond and accept new bonds from new partners. It is from this viewpoint that we describe the molecular environments in water in terms of local and collective field fluctuations. We imagine that there is at least a conceptual separation between the HOD and its proximal hydrogen bonding partner (bonded to H) and the remainder of the liquid.

Experiments and computer simulations[10−12] have found that on molecular length scales water molecules undergo fast (tens of femtoseconds), localized intermolecular vibrations, but on length scales larger than one solvation shell, descriptive variables are no longer molecular in origin. This is the regime of density and polarization fluctuations, where groups of molecules move in concert. Such long-range fluctuations can cause instabilities in a hydrogen bond and force molecules to find new hydrogen bonding partners, thereby reorganizing the local structure.

Competition between localized microscopic motions and cooperative rearrangements are two key players that control chemistry in solution. A specific example where collective motions of water molecules dominate observables that are ostensibly molecular comes from electron transfer and solvation dynamics.[13] In the Marcus scenario, long wavelength electric field fluctuations drive electron transfer and stabilize the reactants and products of a chemical reaction when the participants are adjacent to one another in the liquid host.[13]

Vibrational spectroscopy of the hydride stretch in water has traditionally focused on the role of local hydrogen bonding interactions. The earlier work of Badger[14] and Rundle[15] identified quantitative relationships between the degree of hydrogen bonding and the OH stretch frequency (ω_{OH}), but in 1974, Novak[16] showed that for hydrogen bonding solids there is a strong correlation between the interatomic oxygen−oxygen distance between hydrogen bonded pairs, R_{OO} (Figure 3), and ω_{OH}. Eager to observe hydrogen bond breaking in real time, experimentalists turned to time-resolved transient hole burning (THB), a technique popularized in the studies of structural dynamics in low-temperature glasses and biological photochemistry.[17,18] In these experiments, a narrow band pump pulse saturates a fraction of the molecules in a broad absorption band. Thermal agitation causes molecules to lose memory of their initial environments. When this happens, their frequencies shift and the spectral "hole" fills back up. If the lifetime of the transition is much longer than the time scales for spectral

* Corresponding author. E-mail: tokmakof@mit.edu.

10.1021/jp051364m CCC: $30.25
Published on Web 09/30/2005

diffusion and the dynamics are linear, linear response theory relates the rate of spectral relaxation in a THB experiment to the equilibrium frequency fluctuations.[9]

In 1991, Lauberau published the first IR transient hole burning experiment on the OH stretch of HOD in liquid D_2O, a model system for studying dynamics in water with IR spectroscopy. From his data, he inferred a time scale for single hydrogen bond breaking and multicomponent structural rearrangement because he assigned spectral components to different types of hydrogen bonds.[19] The study reports several time scales for spectral relaxation in water, but the shortest time scale they report is close to their time resolution ($\approx$1 ps). Other THB experiments give a time scale between 500 and $\approx$700 fs for the long time component of spectral diffusion.[20,21] These experiments argued that the 700 fs to 1 ps decay corresponds to the hydrogen bond kinetic making and breaking rate between HOD and its hydrogen bonding partner; however, such an interpretation relies heavily on a strong correlation between the geometrical variables that identify a hydrogen bond and ω_{OH} that is unique and persistent on the time scale so that the hydrogen bond remains intact ($\approx$1 ps). For Laubereau's interpretation to be accurate, there must also be a strong correlation between ω_{OH} and the degree of tetrahedrality in the first solvlation shell of HOD.

Recently, several computational studies on the nonlinear-IR spectroscopy of HOD in liquid D_2O have appeared.[22−27] These studies present a simple picture of vibrational dephasing, where the short time decay arises from fluctuations in the distance between the center of HOD and its hydrogen bonding partner, and the long time relaxation measures hydrogen bond breaking.[24,25] These investigations have argued for an entirely local picture for vibrational spectroscopy in water, where the only important participants are the HOD molecule and its hydrogen bonding partner. A number of studies also have used molecular dynamics (MD) simulations to examine the relationship between R_{OO} and ω_{OH} in the liquid phase. The studies have determined that the correlation between R_{OO} and ω_{OH} remains present but becomes more modest in the liquid;[24,26] however, they ultimately reach the same conclusion that the experimentalists do about the long time decay of frequency fluctuations.

In this report, we develop a highly simplified microscopic model for the spectroscopy of the OH stretch of HOD in liquid D_2O. With this model, we find a reasonably good correlation between the OH frequency and the geometrical hydrogen bonding variables, $\cos(\alpha)$ and R_{OO}, but this correlation is just a manifestation of the much stronger relationship between the frequency and the electric field that the molecules in the liquid impart on the proton. With the exception of the hydrogen bonding partner, molecules in the first solvation shell do not exert a large influence on the OH stretching frequency. Thus, IR experiments on the OH stretch are not sensitive to specific dynamics of hydrogen bonding partners not directly bonded to the proton. We conclude that electric field fluctuations drive the loss of vibrational coherence at all times. At short times, these fluctuations reflect changes in local geometries between HOD and its hydrogen bonding partner. Of course, local geometrical reconfigurations are not independent from larger length scale polarization and density fluctuations that dominate relaxation on picosecond time scales. Electrostatics couple these two relaxation mechanisms. The vibrational dephasing of HOD in liquid D_2O closely resembles Marcus' picture of electron transfer.[13] Our picture is highly suggestive of a reduced model for the vibrational spectroscopy of water, where the only essential molecular feature is the hydrogen bonding interaction between HOD and a single neighbor.

II. Methods

To relate vibrational frequency to microscopic coordinates, we developed an atomistic model that makes suitably accurate predictions for vibrational spectroscopies but retains a faithful description of the bulk and structural properties of the liquid. We used a conventional water potential (SPC/E)[28] to model the translations and rotations of the water molecules. The SPC/E[28] model of water places point charges on each of the atomic positions to mimic the averaged electronic distribution, and a Lennard-Jones site resides on the center of the oxygen atom to provide an excluded molecular volume. Simulations using this potential reproduce thermodynamic, bulk transport, and structural data for water with marked accuracy, including the diffusion constant, liquid−vapor coexistence line, and low frequency dielectric constant. Because the vibrational temperature for the hydride stretches and bends is large, we maintained the conventional use of the potential by keeping all intramolecular distances and angles rigid but modified the potential to introduce the OH stretch as a single quantum mechanical degree of freedom.

The OH oscillator Hamiltonian must describe the vibrational spectrum in the absence of any environmental coupling, so we used a local mode gas-phase Hamiltonian[29] for the vibration. Formally, the vibrational Hamiltonian contained three internal coordinates, one for each of the hydride stretches and one for the bend. The dominant intramolecular coupling in this representation is kinetic, which is proportional to the dot product of the conjugate momenta for each internal coordinate divided by the atomic masses. One can safely ignore these perturbations because these coordinates are nearly orthogonal. The inverse mass-weighting further diminishes the importance of the kinetic couplings[29] relative to the environmental perturbations of the solvent. Within these approximations, the vibrational Hamiltonian is one-dimensional.

A. Calculating Vibrational Frequencies. One can partition the total Hamiltonian by separating the quantum mechanical OH oscillator, or system coordinate, from all of the classical, or bath, degrees of freedom. The Hamiltonian acquires an additional term that couples the system and bath coordinates. The total Hamiltonian is

$$H = H_s(\{P\},\{Q\}) + H_{sb}(\{p\},\{q\},\{P\},\{Q\}) + H_b(\{p\},\{q\}) \quad (1)$$

Here, $\{P\}$ and $\{Q\}$ are the momenta and the atomic displacements of the vibrations in internal coordinates, and $\{p\}$ and $\{q\}$ are the generalized classical momenta and the coordinates for the rigid body motion of the water molecules. The bath Hamiltonian H_b describes the translations and rotations of the molecules in the liquid, or the slow coordinates. The coordinates $\{q\}$ and momenta $\{p\}$ come from a MD simulation of H_b. H_s, the system Hamiltonian, describes the vibrational spectrum of the isolated molecule. These vibrations are faster than the coordinates of the bath Hamiltonian, so H_s is a function of the fast degrees of freedom, $\{P\}$ and $\{Q\}$. It has eigenstates, $|a\rangle$, that satisfy the Schrödinger equation,

$$H_s|a\rangle = \epsilon_a|a\rangle \quad (2)$$

The potential energy surface of the isolated HOD molecule is anharmonic in the internal coordinates, $\{Q\}$. The local mode description accurately models the anharmonicities of the potential energy surface and treats the kinetic couplings perturbatively. We ignored the kinetic couplings because, for HOD, these couplings are significantly smaller than those between the vibration and the molecules in the liquid. With these approxima-

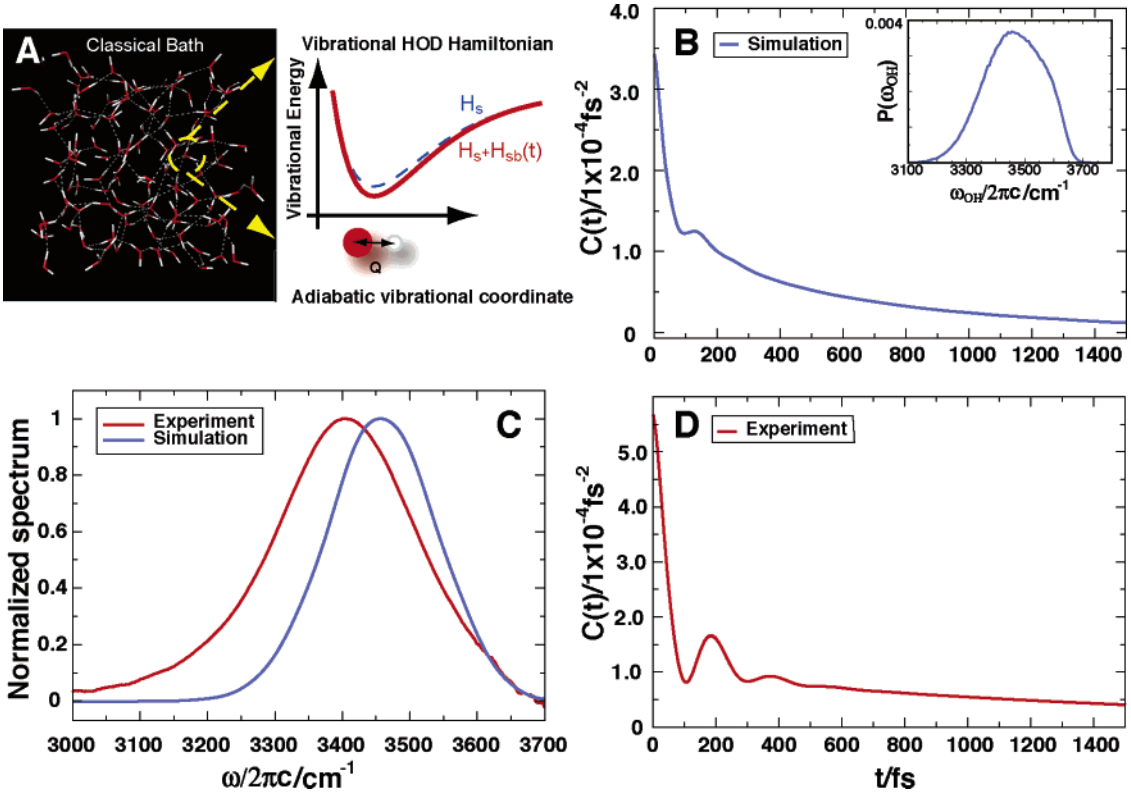

Figure 1. (A) Schematic of the adiabatic separation used to compute the spectroscopy of HOD in liquid D_2O and a comparison to the experimental data for both the correlation functions (B) and (D) and the IR absorption line shape (C). The line shape is ≈190 cm^{-1} wide (fwhm) and exhibits some of the asymmetry in the experimental absorption experiment; however, it falls nearly 70 cm^{-1} short of describing the quantitative spectral line width and is shifted roughly 30 cm^{-1} to the blue. The narrow spectral width is due partly to the underestimation of the width for the equilibrium probability distribution function of ω_{OH} and $P(\omega_{OH})$, displayed in the inset to (B). The correlation functions have a sharp intial drop, a beat, and a long time decay.

tions, H_s is a one-dimensional Morse oscillator with eigenfunctions $\langle x|a\rangle$ given by generalized Laguerre polynomials.[30] These functions are the basis set for perturbation theory.

The system−bath Hamiltonian, H_{sb}, couples the vibration to the slower translations and rotations of the bath molecules. For a given configuration of the bath variables, the total potential energy of the system is a function of Q. Often, the most practical and computationally efficient way to find H_{sb} is to fix the bath variables and expand the total Hamiltonian as a Taylor series in the internal coordinates (and possibly momenta) and then quantize them[31] in the adiabatic basis set. H_{sb} is usually a slowly varying function of the system coordinates, and a low-order approximation, usually first- or second-order, is a good approximation. We truncate the expansion at second order in Q so that the approximate system−bath Hamiltonian becomes

$$H_{sb} = FQ + GQ^2 \tag{3}$$

To build the Q and Q^2 matrices, we used parameters from the local mode Hamiltonian of Reimers and Watts[29] and numerically integrated the eigenfunctions from Watson et al.[30] Figure 1A is a diagram of the adiabatic scheme. We have chosen a notation that is commensurate with Oxtoby's,[31] where F is the derivative of the potential energy at $Q = 0$, keeping the center of mass for the vibration fixed.

$$F = \frac{\partial V_{SPC/E}(Q,\{\mathbf{r}\})}{\partial Q} = -\mu\hat{\mathbf{r}}_{OH}\cdot\left(\frac{\mathbf{F}_O}{m_O} - \frac{\mathbf{F}_H}{m_H}\right) \tag{4}$$

$\mathbf{F}_O$ is the force on the oxygen (hydrogen) atom, m_O is the mass of the oxygen (hydrogen) atom, $\mathbf{r}_{OH} = (\mathbf{r}_O - \mathbf{r}_H)/(|\mathbf{r}_O - \mathbf{r}_H|)$, and μ is the reduced mass of O and H. Computing F for each configuration of the simulation is straightforward in the Velocity−Verlet algorithm because one stores the forces at each time step of the simulation. Calculating G requires an additional cost, equivalent to the force loop. Analytical expressions for G appear in the Appendix.

The first and second terms of F are the (mass-weighted) bath-induced forces on the oxygen and hydrogen atom, respectively, in the direction of the OH bond. In general, the magnitude of the OH component of the force for the hydrogen is comparable to that of the oxygen, but the inverse mass-weighting makes the second term larger. The forces on the hydrogen are purely electrostatic, so the vibrational frequency is manifestly sensitive to the electric field evaluated at the proton. The dot product with $\hat{\mathbf{r}}_{OH}$ implies that electric fields in the direction of the OH bond make F the largest and hence are most effective at inducing frequency shifts.

Once we have the system-bath Hamiltonian, we solve the time-independent Schrödinger equation for the vibrational eigenstates for the frozen or clamped configuration of the slow variables at time t, $\mathbf{r}(t)$.

$$H|\Psi[\mathbf{r}(t)]\rangle = \mathcal{E}[\mathbf{r}(t)]|\Psi[\mathbf{r}(t)]\rangle \tag{5}$$

The adiabatic solutions $|\Psi[\mathbf{r}(t)]\rangle$ are coherent superpositions of the unpreturbed states,

$$|\Psi[\mathbf{r}(t)]\rangle = \sum_n c_n(t)|n\rangle \tag{6}$$

The coefficients carry the time dependence,

$$c_n(t) = \langle n|U(t)|\Psi[\mathbf{r}(0)]\rangle \tag{7}$$

To calculate spectroscopic signals, we assume that the perturbation is weak enough so that it does not induce transitions between the unperturbed states. This amounts to making the "pure dephasing" approximation that replaces the full time evolution operator, $U(t)$, with its projected diagonal part, $U(t) \approx \sum_n |n\rangle\langle n|U(t)|n\rangle\langle n| \equiv U_n(t)$. The pure dephasing approximation to $U(t)$ from eq 5 is

$$U_n(t) = \sum_n |n\rangle\langle n| \exp\left[-\frac{\mathrm{i}}{\hbar}\int_0^t \mathrm{d}t' \mathscr{O}_n(\mathbf{r}(t'))\right] \tag{8}$$

Energy differences between vibrational states from eq 5 describe spectral diffusion. Specifically, the OH frequency is the fundamental transition $\hbar\omega_{\mathrm{OH}}(t) = \mathscr{O}_1(\mathbf{r}(t)) - \mathscr{O}_0(\mathbf{r}(t))$, where the subscripts denote the vibrational quantum state where the energy is evaluated. If the frequency fluctuations are Gaussian and fluctuations between levels and transition dipole moments are harmonic,[32] vibrational third-order response functions depend solely on the frequency autocorrelation function, $C_{\omega\omega}(t) = \langle \delta\omega_{\mathrm{OH}}(t)\, \delta\omega_{\mathrm{OH}}(0)\rangle$, and $\delta\omega_{\mathrm{OH}}(t) = \omega_{\mathrm{OH}}(t) - \langle\omega_{\mathrm{OH}}\rangle$.

In this manuscript, we use second-order time-independent perturbation theory to approximately diagonalize H_{sb}. To second order, the vibrational energies are

$$\mathscr{O}_n^{(2)} = \langle n|H_{\mathrm{sb}}|n\rangle + \sum_{k,n\neq k} \frac{|\langle n|H_{\mathrm{sb}}|k\rangle|^2}{\epsilon_n - \epsilon_k} \tag{9}$$

Here, $|n\rangle$ and ϵ_n are the unperturbed states and energies, respectively. The second-order term is usually smaller than the first-order term, so first-order perturbation theory is reasonably accurate. First-order perturbation theory provides simple expressions for the vibrational frequency shifts.[32] Furthermore, differences in the diagonal matrix elements for $\mathbf{Q}^2$ are smaller than those for Q for low-lying vibrational states. If we neglect the G term in eq 3 and ignore the forces on the oxygen atom, the system-bath Hamiltonian is

$$H_{\mathrm{sb}} \approx z_{\mathrm{H}} Q E$$
$$E \equiv \hat{\mathbf{r}}_{\mathrm{OH}} \cdot \mathbf{E} \tag{10}$$

where the electric field $\mathbf{E}$, appearing in eq 10, is that generated by all the molecules in the simulation and their periodic images. z_{H} is the charge of the proton. At this level of approximation, H_{sb} is isomorphic with the first-order Stark shift Hamiltonian,

$$H_{\mathrm{Stark}} = -\boldsymbol{\mu}\cdot\mathbf{E} \tag{11}$$

which can be seen by making the substitution

$$-\boldsymbol{\mu}\cdot\mathbf{E} = z_{\mathrm{H}} Q \hat{\mathbf{r}}_{\mathrm{OH}}\cdot\mathbf{E} \tag{12}$$

We are using the self-consistent mean field method of adiabatic quantum mechanics[33] but neglecting the forces of the quantal degree of freedom on the slow variables. One can solve for these forces by applying the Hellmann−Feynman theorem to the matrix elements of H_{sb} with the adiabatic quantum states in eq 5,

$$\mathscr{F}_i(t) = \langle \Psi[\mathbf{r}(t)]|(-\nabla_i H_{\mathrm{sb}})|\Psi[\mathbf{r}(t)]\rangle \tag{13}$$

Here, $\mathscr{F}_i(t)$ is the force from the quantum mechanical OH vibration on atom i and ∇_i is the gradient with respect to the position of atom i. Omitting the Hellmann−Feynman forces is standard practice,[27,31,34] but it means that the expectation value of the total Hamiltonian is not a constant of the motion. When the Hellmann−Feynman forces are neglected, H_{s} and H_{b} conserve energy in the adiabatic scheme trivially but H_{sb} does not. The standard deviation of the energy violations is $\langle H^2\rangle - \langle H\rangle^2 = \langle H_{\mathrm{sb}}{}^2\rangle$. The actual value depends on the state of the oscillator, but the more meaningful quantity is the difference between the Hellmann−Feynman force on atom i when the oscillator is in the ground compared to this force when it is in the first vibrationally excited state. The distribution of work that the oscillator does on the solvent when it is promoted to the first excited state is given roughly by the distribution of ω_{OH} (inset of Figure 1B), and the width of it is related to the vibrational Stokes shift.[23] The standard deviation of this distribution is $\approx$100 cm^{-1}, or about half of $k_{\mathrm{B}}T$. We plan to address this issue by including the Hellmann−Feynman forces in a future publication.

The Stokes shift is related to the difference in solvation free energy between a molecule in the ground state and in the excited state. This energy has both electronic and vibrational parts. Including the Hellmann−Feynman forces between the oscillator and the solvent would treat the vibrational part, but because the electronic degrees of freedom in the SPC/E potential are fixed, we cannot capture the electronic part. Although the Stokes shift of our system is on the order of $k_{\mathrm{B}}T$, it is approximately an order of magnitude smaller than that obtained from studies that examined the electronic solvation dynamics of a chromophore in water.[35] Electronic excitation often significantly changes the electronic structure of the molecule and can make nonpolar electronic chromophores polar in the excited state.[35] Even though the anharmonicity of the OH stretch is large, vibrational excitation only occurs among the first three levels in a third-order nonlinear-IR experiment. Excitation among these levels should only induce a small perturbation on the molecular electronic structure. The fact that the Stokes shift inferred from experiments[20] is similar to that predicted from simulation[23] supports this notion.

Our simulations neglected the processes of vibrational relaxation and energy transfer. Unfortunately, serious fundamental inconsistencies arise when one attempts to compute energy transfer rates between classical and quantum degrees of freedom.[36] Although improvised protocols exist for calculating these rates based on Landau and Teller's formula,[37] a more satisfactory calculation likely requires elaborate quantum or semiclassical dynamical rules that are beyond the scope of the current study. Recent experiments find a vibrational relaxation and energy redistribution time of around 700 fs.[38] We expect the consequences of neglecting vibrational energy redistribution to become most severe after this time scale.

B. Simulation Details. We performed molecular dynamics simulations of one HOD and 107 D_2O molecules by repeated integration of Newton's equation of motion using the Velocity−Verlet algorithm[39] with a 3-fs time step and by applying periodic boundary conditions to the molecular centers of mass. This time step kept the energy fluctuations to $\approx 10^{-4}$ of $\langle H_{\mathrm{b}}\rangle$. We used the SPC/E potential[28] for the bath dynamics. The RATTLE algorithm[39] kept all bonds in the molecules rigid. The room-temperature thermodynamic state point corresponds to a density of 1.117 g/cm^3 and a temperature of 298 K. Because we are not solving the equations of motion exactly, the velocities need to be periodically rescaled to match the kinetic energy at eqilibrium. By rescaling the velocities every 10 ps, we kept the kinetic energy near the equilibrium thermal value and ensured that the rescaling interval was approximately an order of

magnitude longer than that for dynamics of interest. Accurate calculation of dielectric properties requires careful treatment of the long-range electrostatics that we computed using Ewald summation.[39]

We identified the first solvation shell as the four nearest neighbors surrounding the HOD molecule. Out of these, we determined the hydrogen bonding partner by selecting the largest value of cos(α) out of the four nearest neighbors. This selection strategy allows one to assign a hydrogen bonding partner even during transient fluctuations away from a hydrogen bond.

III. Results

To ensure that our atomistic strategy for computing vibrational frequencies captures essential features of vibrational spectroscopy, we compare $C_{\omega\omega}(t)$ and the absorption line shape to recent experiments.[32] The absorption spectrum is proportional to the Fourier transform of the dipole−dipole correlation function.[40,41]

$$\sigma(\omega) \propto \omega \int_{-\infty}^{\infty} \mathrm{d}t\, \mathrm{e}^{\mathrm{i}\omega t} \langle \boldsymbol{\mu}(t)\cdot\boldsymbol{\mu}(0)\rangle \tag{14}$$

The time-evolution operator from eq 8 yields the OH absorption line shape in the adiabatic picture as

$$\sigma(\omega) \propto \omega \int_{-\infty}^{\infty} \mathrm{d}t\, \mathrm{e}^{\mathrm{i}\omega t} \left\langle \exp\left[-\frac{\mathrm{i}}{\hbar}\int_0^t \mathrm{d}t' \mathcal{O}_1(\mathbf{r}(t')) - \mathcal{O}_0(\mathbf{r}(t'))\right]\right\rangle \langle \mathbf{e}(t)\cdot\mathbf{e}(0)\rangle \mathrm{e}^{-t/2T_1} \tag{15}$$

In eq 15, $\mathbf{e}(t)$ is the unit vector of the OH bond at time t. The vibrational lifetime T_1 is included as an empirical factor that represents how the flow out of the population $|1\rangle\langle 1|$ affects the coherence $|0\rangle\langle 1|$. The numerical value of T_1 that we have used comes from recent pump−probe experiments[38,42] and is 700 fs. The averages over the vibrational state of the molecule and the rotational states of the molecule are independent because we did not include ro-vibrational coupling.

The line shape computed from the simulation is roughly the same shape as the experimentally measured one but is ≈70 cm^{-1} too narrow (fwhm). The reason for the discrepancy most likely lies in the width of the frequency distribution. This distribution is 265 cm^{-1} wide (inset to Figure 1B), so spectral diffusion can only narrow it. The experimental $C_{\omega\omega}(t)$ evaluated at $t = 0$ provides an estimate for the mean squared value of the distribution that is nearly 60% larger than that computed from the simulation.

The correlation function from simulation decays, initally with a fast time constant of 35 fs, has a beat that peaks near 125 fs and has a long time decay of ≈600 fs. Figure 1 compares the experimental and simulated $C_{\omega\omega}(t)$. The correlation function extracted from the experiment decays with a fast time constant, exhibits a beat that peaks at 180 fs, and has a long time decay of 1.4 ps. Given the simplicity of our approximations, the agreement between experiment and simulation in Figure 1 for both the absorption spectrum and $C_{\omega\omega}(t)$ is notable. Because there have been several different approaches to computing the IR line shape and $C_{\omega\omega}(t)$ with classical molecular dynamics potentials that all achieve similar results, the disagreement between the simulation and experiment probably does not highlight a problem with the adiabatic approach to the frequency calculation itself.[22,26] There are several approximations that one has to make to extract $C_{\omega\omega}(t)$ from the experiment. Strictly speaking, the IR3PEPS experiment can only extract $C_{\omega\omega}(t)$ reliably when the pulses have infinite bandwidths, the frequency fluctuations obey Gaussian statistics, and the lifetime of the excited state is very long on the time scale of frequency fluctuations. These approximations are not quite satisfied for HOD in D_2O. Of course, the SPC/E potential that we have used has been parametrized to reproduce bulk quantities in water and may not be quantitatively accurate for vibrational spectroscopy. Atomistic models based on simple strategies nonetheless reproduce many qualitative features in $C_{\omega\omega}(t)$ and give an explicit microscopic model that we use to analyze the vibrational spectroscopy of HOD in liquid D_2O.

Equipped with an explicit microscopic model, we examine the relationship between frequency and molecular hydrogen bonding environments. Our analysis proceeds by defining a set of physically motivated order parameters that classify the liquid environment. We then look for statistical correlations between these order parameters and ω_{OH}. After establishing the statistical significance of our chosen order parameters, we identify a set of relevant order parameters, those that are strongly correlated with ω_{OH}, and then compare the characteristic time scales of frequency fluctuations to those of the relevant order parameters.

A. Role of the Hydrogen Bonding Partner. Our atomistic model allows us to explore the connection between ω_{OH} and a hydrogen bonding structure in detail. Let us suppose that one could select a distribution of molecules by labeling them with a short pulse laser that has arbitrary time and frequency resolution. Figure 2 is a three-dimensional plot of the probability density of the atomic positions for the hydrogen bonding partner on the red, middle, and blue sides of the absorption line, calculated from our simulations. Each column in Figure 2 is the collection of molecules in a 50 cm^{-1}wide bin about the selected frequencies (3300, 3450, and 3600 cm^{-1}). Isosurfaces represent the full width at half-maximum surface for the atomic density of the hydrogen bonding partner's hydrogen (white) and oxygen (red) atoms. Progressing from the red side of the line to the blue side of the line, the oxygen density goes from being tightly localized to being diffuse. All the surfaces seem to exhibit nearly azimuthal symmetry about the OH bond. The hydrogens of the nearest neighbor point away from the HOD molecule and do not significantly shift the frequency on the red or the middle of the band. For these regions of the spectrum, the shapes of the distributions of the neighbors' hydrogen atoms are similar. On the blue side of the line, however, the hydrogen atoms of the hydrogen bonding partner become more important, filling the space that the oxygen atom does in the strongly hydrogen bonded case. We imagine that the structure that these densities depict comes from a progressive weakening of hydrogen bonds in moving from the red side to the blue side. It is obvious from these surfaces that R_{OO} is not the only coordinate that determines ω_{OH}. Moving from red to blue, the correlation with the hydrogen bonding angle, α, becomes more significant as R_{OO} becomes less significant. A successful variable that describes the relationship between ω_{OH} and the local intermolecular structure must at least be a function of R_{OO} and α.

Recall that R_{OO} and α are convenient descriptors of hydrogen bonding in computer simulations. To examine the relationship between hydrogen bonding coordinates and the frequency, we computed joint probability distributions of ω_{OH} and local hydrogen bonding variables R_{OO} and cos(α). Figure 3 shows the results. We calculated the joint probability distributions by making bivariate histograms of the order parameters and ω_{OH}. The correlation coefficient,

$$\rho = \frac{\langle (x - \langle x\rangle)(\omega_{OH} - \langle \omega_{OH}\rangle)\rangle}{\sqrt{\langle (x - \langle x\rangle)^2\rangle \langle (\omega_{OH} - \langle \omega_{OH}\rangle)^2\rangle}} \tag{16}$$

quantifies the staistical correlation between a chosen order

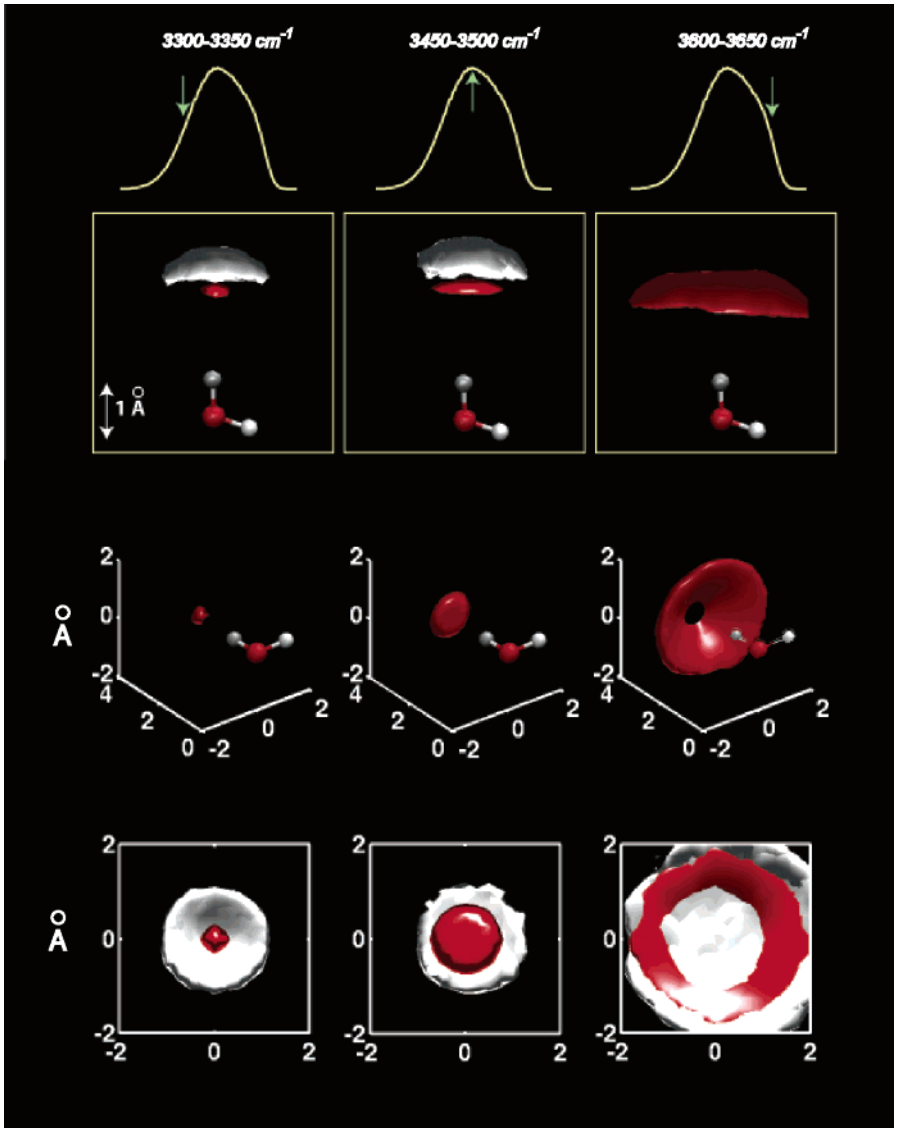

Figure 2. Still lifes of hydrogen bonded configurations visualized through the OH frequency. This plot shows atomic probability densities of HOD's nearest hydrogen bonding partner for various ranges of ω_{OH}. Surfaces represent the full width at half-maximum of the atomic probability density for the neighbor's hydrogens (white) and oxygens (red). The first row is the distribution of $\omega_{OH}/(2\pi c)$, which peaks at 3450 cm^{-1} and is 265 cm^{-1} wide (fwhm). The arrows designate the OH frequency for each column. Numbers on the axes are distances in Å for a coordinate system centered on HOD's oxygen atom. The fourth row shows the distribution of molecular configurations, viewed from the perspective of the OH bond. Spectral diffusion of ω_{OH} is the time evolution over molecular geometries, depicted in this figure. The blue side of the line shows cleaved or severely strained hydrogen bonds. Clearly, ω_{OH} is not a simple function of R_{OO} for all frequencies.

parameter x and ω_{OH}. If ω_{OH} is a linear function of x, then $\rho^2 = 1$. ρ is normalized to -1 for anticorrelated variables and to $+1$ for perfectly correlated ones. $\rho = 0$ can indicate statistical independence of x and ω_{OH}.

The statistical correlation between R_{OO} and ω_{OH} is reasonably strong ($\rho = 0.77$) but weakens at higher values of frequency and OH···O distance. Several researchers have examined this relationship in detail with several different models and approaches to the frequency calculation.[24,26,43] Their results are virtually identical to those displayed in Figure 3B. Comparing Figure 3 with the predictions from Novak's[16] crystalline data suggests that the loss of the sharp correlation between R_{OO} and ω_{OH} in the liquid comes from the higher degree of molecular disorder in the liquid. In the liquid state, molecules explore larger hydrogen bonding angles (α) than they do in the crystal phase. Figure 3 shows that, as R_{OO} becomes larger, deviations in the polar angle, α, are more severe, weakening the hydrogen bond.

We chose to focus on probability per unit of $\cos(\alpha)$ because the spatial volume corresponding to a small interval in $\cos(\alpha)$ is independent of α. As a result, $P(\omega_{OH},\cos(\alpha))$ is proportional to the average spatial density of the hydrogen atom at polar angle α for a given value of ω. Such a spatial density directly reflects the distribution of hydrogen bonding geometries, shown in Figure 2. The spatial volume corresponding to a small interval in α, on the other hand, is proportional to $|\sin(\alpha)|$. This can be seen from the Jacobian that relates the two probability densities

$$P(\cos(\alpha),\omega_{OH})\, d(\cos(\alpha))\, d\omega_{OH} = P(\alpha,\omega_{OH})|\sin(\alpha)|\, d\alpha\, d\omega_{OH} \quad (17)$$

For any nonsingular probability density, $P(\alpha,\omega_{OH})$ must vanish at $\alpha = 0$. The fact that $P(\omega_{OH},\alpha)$ peaks at nonzero α does not suggest that energy is minimized when hydrogen bonds are slightly bent. To the contrary, the peak of $P(\omega_{OH},\cos(\alpha))$ verifies that the most probable hydrogen bonding configuration is linear for any value of $\omega_{OH} < 3450$ cm^{-1}.

B. First Solvation Shell and Tetrahedrality. Ice is a honeycomb network of strong hydrogen bonds, where each

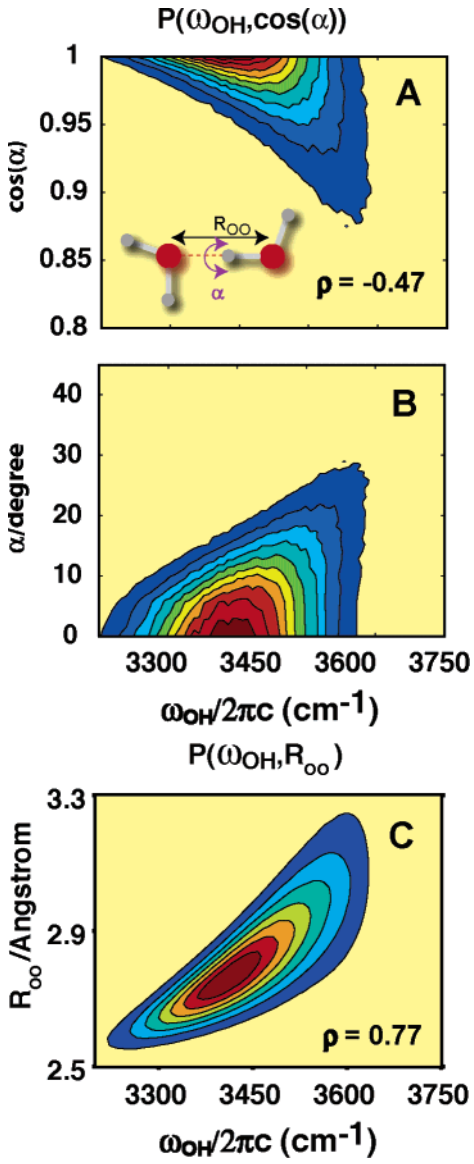

Figure 3. Joint probability distribution for intermolecular hydrogen bonding variables R_{OO} and cos(α) with ω_{OH}. The geometrical criterion for hydrogen bonding identifies hydrogen bonded pairs on the basis of the values of R_{OO} and cos(α). Part A defines α and R_{OO} and displays $P(\omega_{OH},\cos(\alpha))$. The correlation coefficient is −0.47. Part B is a linear interpolation of $P(\omega_{OH},\cos(\alpha))$ to linear spacing in α. It does not contain the Jacobian for the transformation and hence is nonzero at α = 0. (C) R_{OO} shows the stronger correlation to ω_{OH}, with $\rho = 0.77$, than does cos(α) in part A. At higher values of ω_{OH}, the correlation between ω_{OH} and R_{OO} grows weaker whereas that between ω_{OH} and cos(α) becomes stronger.

molecule donates and accepts two bonds. In the liquid state, tetrahedral order persists[44] on the length scale of one solvation shell, but longer range crystalline order disappears. The vibrational absorption spectrum of the OH stretch is slightly different in water and ice. In hexagonal (I_h) ice, the IR spectrum is broader and shifted to the red with respect to the liquid. This fact led Laenen and Laubereau[45,46] to hypothesize that the value of ω_{OH} describes the ordering, or degree of tetrahedrality, in the first solvation shell. We examined this hypothesis by looking at the joint probability distribution of ω_{OH} with the tetrahedrality order parameter, q, defined as

$$q = 1 - \frac{3}{8}\sum_{j=1}^{3}\sum_{k=j+1}^{4}\left(\cos(\theta_{jk}) + \frac{1}{3}\right)^2 \qquad (18)$$

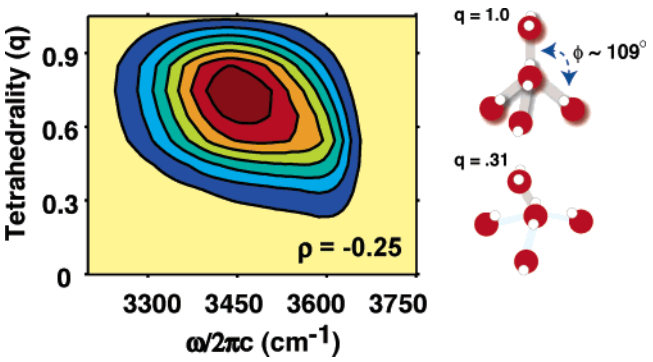

Figure 4. Joint probability distribution of tetrahedrality and OH frequency. The poor correlation demonstrates that the OH frequency is not a sensitive probe of local tetrahedral order in water. The illustration on the right shows the numerical value of the order parameter in a perfect tetrahedron and a disjoint, though mostly tetrahedral, configuration. Typical values for q in the liquid lie between 0.5 and 0.9.[44]

where the unit vectors point from the oxygen of HOD to those of the first solvation shell molecules j and k.[44] If the first solvation shell forms a perfect tetrahedron about HOD, $q = 1$. The average of q approaches zero in a dilute gas that prefers no local order. Typical values in the liquid range from 0.5 to 0.9.[44] Figure 4 shows that there is negligible correlation between the OH frequency and the degree of tetrahedrality in the first solvation shell.

C. Electric Field Order Parameters. The hydrogen bonding variables R_{OO} and cos(α) correlate reasonably well with ω_{OH}. However, as Figure 2 suggests, it is possible to devise a function of these variables that exhibits an even stronger correlation with ω_{OH}. To isolate the specific contribution of the hydrogen bonding partner, we defined the electric field order parameter E_0 to be its electric field at the proton in the direction of $\hat{\mathbf{r}}_{OH}$. E_1 is the analogous quantity for all molecules in the first solvation shell.[32] It is also useful to define the "collective" electric field, E_c, as the field on the proton from all molecules except the hydrogen bonding partner by making the following decomposition,

$$E_c = E - E_0 \qquad (19)$$

Figure 5 shows the joint probability densities for the electric field order parameters. E_0 is more strongly correlated to ω_{OH} than either R_{OO} or cos(α) ($\rho = 0.89$). Adding molecules in the first solvation shell shifts the position of the maximum of the joint probability density but does not improve the correlation.

Figure 2 shows that, on the red side and in the middle of the frequency distribution, the hydrogen atoms of the hydrogen bonding partner point away from the HOD molecule. Because the hydrogen densities for the red and the middle of the frequency distribution are so similar, we can conclude that the hydrogen atoms are not important for determining the frequency in these regions of the spectrum. In these regions, the oxygen atom dominates the electric field at the proton and it is easy to express E_0 in terms of ω_{OH} and cos(α). When working in units where the OH bond has a length of unity (Å for SPC/E), we obtain

$$E_0 \propto \frac{R_{OO}\cos(\alpha) - 1}{(R_{OO}^2 + 1 - 2R_{OO}\cos(\alpha))^{3/2}} \qquad (20)$$

On the blue side of the line, the hydrogen atoms of the nearest neighbor begin to play a more pronounced role in perturbing

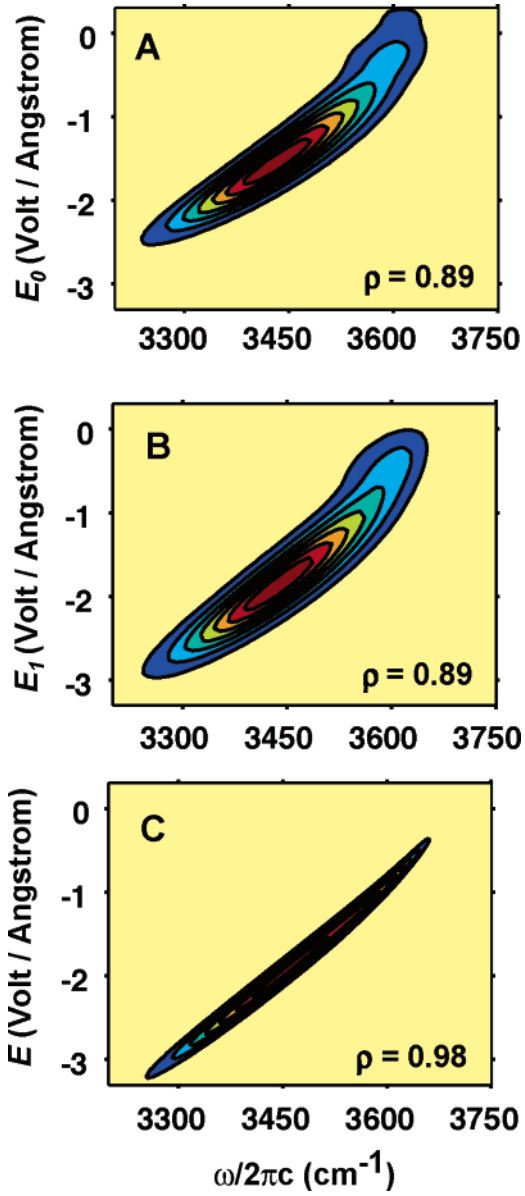

Figure 5. Joint probability densities of electric field variables and ω_{OH}. (A) The electric field from the nearest neighbor ($\mathbf{E}_0$) is a function of the intermolecular geometries investigated in Figure 3 but improves the correlation between ω_{OH} and either R_{OO} or cos(α) alone. (B) Inclusion of the electric field from all the molecules in the first solvation shell shifts the position of the maximum of the probability density, but it does not improve the correlation. (C) By including the electric field from all molecules in the simulation and their periodic images, the correlation coefficient nears unity.

ω_{OH}. For these configurations, the approximate system-bath Hamiltonian is a dipole−dipole interaction between the dipole of the hydrogen bonding partner and the Stark dipole (eq 11) of HOD. This interaction introduces extra intermolecular variables, and there is no simple relationship between E_0, R_{OO}, and cos(α). These diverse configurations seen in Figure 2 distort the probability distributions in Figure 5A,B on the blue side.

Another simple electrostatic argument explains the weak dependence of ω_{OH} on tetrahedrality (q). The OH bond is one leg of the hydrogen bonded tetrahedron in the first solvation shell. The remaining three legs of the tetrahedron are nearly orthogonal to the OH bond, with an angle of ≈109°. Equation 10 selects the component along the direction of the OH bond. As a result, the relative contribution to the frequency shift of the remaining molecules in the first solvation shell relative to

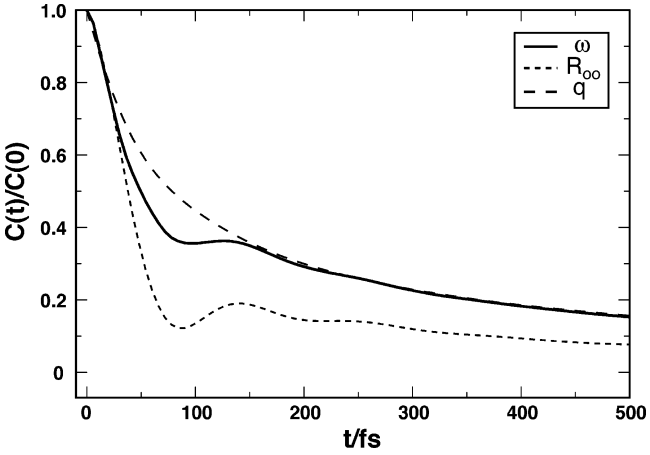

Figure 6. Dynamics of molecular order parameters. As one would anticipate from the weak correlation between q and ω_{OH}, the dynamics of q do not follow the dynamics of ω_{OH} at short times. The beat in $C_{\omega\omega}(t)$ is most pronounced in R_{OO}.

that from the nearly collinear hydrogen bonding partner is diminished. The OH frequency is so sensitive to the hydrogen bonding partner that it is an insensitive probe of the remainder of the molecular structure in the first solvation shell.

D. Dynamics. IR spectroscopy measures response functions that in perturbative limits can be expressed in terms of equilibrium time correlation functions (TCFs), such as $C_{\omega\omega}(t)$.[41] These equilibrium TCFs are the connection between simulation and experiment and describe the time scales of natural fluctuations at equilibrium. Because intermolecular motions in water are fast (≈100 fs), building intuition about vibrational spectroscopy based on joint probability densities alone can be misleading. Plots such as Figure 2 are instructive to motivate a set of meaningful order parameters but cannot not be relied on to provide a comprehensive picture of vibrational spectroscopy because they ignore the dynamics of molecular environments.

Understanding the spectroscopy in terms of molecular motions lies in quantifying the relationship between the *dynamics* of the relevant order parameters and the frequency. Joint probability distributions and statistical correlations of the statics identified a set of relevant order parameters, E_0, E_c, E, and R_{OO}. Figure 6 is a plot of the normalized TCFs for R_{OO} and q for times less than 500 fs. As q correlates poorly with frequency, the dynamics of q do not follow the dynamics of ω_{OH}. The correlation function in R_{OO}, the interatomic oxygen distance, displays a more pronounced beat than in $C_{\omega\omega}(t)$.

E correlates strongly with ω_{OH}, and its TCF bears remarkable resemblence to $C_{\omega\omega}(t)$. Figure 7 highlights the short time part of the normalized correlation functions for the electric field order parameters. The local field correlations $\langle \delta E_0(t)\, \delta E_0(0)\rangle$ display the same beat at ≈125 fs seen in $C_{\omega\omega}(t)$. The reason is that the local field component in the direction of the OH bond is nearly parallel to the displacement of R_{OO}. The local electric field fluctuations between HOD and its hydrogen bonding partner produce the beat in $C_{\omega\omega}(t)$, but their molecular origin is the hydrogen bond vibration between oxygen atoms.

The beat in $C_{\omega\omega}(t)$, $\langle \delta E_0(t)\, \delta E_0(0)\rangle$, and R_{OO} is also present in the velocity−velocity autocorrelation function of water. Analysis of the velocity−velocity autocorrelation function has revealed that the beat corresponds to density fluctuations in the liquid that behave more like those of a disordered solid than those of a liquid. The "fast speed of sound" in water occurs near the beat frequency and is about twice as fast as the speed of sound of water in the hydrodynamic regime. The fast speed

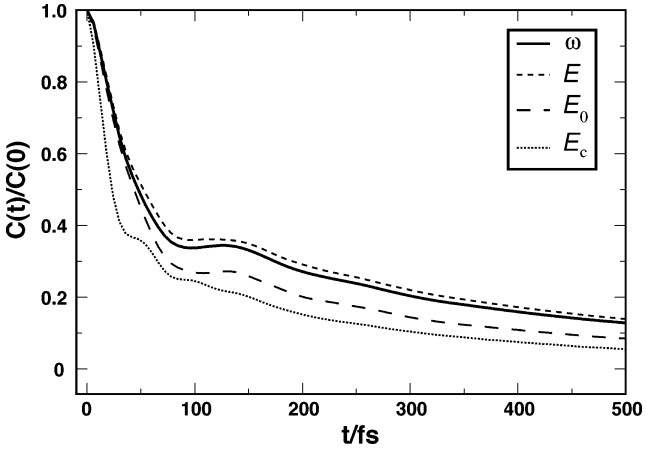

Figure 7. Dynamics of order parameters based on the electric field at the proton. Fluctuations along the hydrogen bond control the relaxation before ≈200 fs. The fluctuations of the local field follow $C_{\omega\omega}(t)$. The collective electric field fluctuations resemble the dielectric response of water. A shoulder appears near ≈60 fs from molecular librations outside the first solvation shell.

of sound in water corresponds to fluctuation wavelengths of ≈3−8 Å.[1,8,47−49] This peculiar behavior can occur in simple liquids too, but in liquid water at ambient conditions, it is fostered by hydrogen bonding.[47,48] A pair of hydrogen bonded water molecules balance the attractive electrostatic forces between the accepting oxygen and the donating hydrogen against the repulsive steric forces that keep molecules apart. The most probable intermolecular oxygen separation at equilibrium is less than the minimum of the steric potential. At the frequency of the beat, the repulsive interactions of oxygen atoms dominate the density fluctuations and give rise to an unusually high Einstein frequency and an underdamped oscillation.[8,47−49] Microscopically, these motions look like a stretch along R_{OO}.

The collective electric field fluctuations $\langle \delta E_c(t)\, \delta E_c(0)\rangle$ exhibit a shoulder at ≈60 fs from librational motions. The shape of this function is remarkably similar to what Lang et al.[11,50] have measured for the solvation correlation function of an electronic chromophore in water. Additionally, Song and Chandler[50] have shown that, for simple solute geometries, the solvation polarization response resembles the collective electric field fluctuations displayed in Figure 7. This observation further supports the notion that for vibrational spectroscopy of HOD in liquid D_2O the prominent molecular feature is the hydrogen bonding partner. The remaining electric field fluctuations follow the dielectric relaxation of a linearly polarizable medium surrounding HOD and its hydrogen bonding partner.

Figure 8 focuses on the long time decay of the normalized TCFs for ω_{OH} and each of the order parameters. The long time (>200 fs) exponential decay time is nearly the same (≈600 fs) for all of these functions, yet many of the order parameters are qualitatively different. For example, the tetrahedrality, which shows poor statistical correlation with the frequency and exhibits different short time dynamics than frequency fluctuations, decays with the same long time constant as that of $C_{\omega\omega}(t)$. The similarity in the decay after ≈200 fs for such different measures of the molecular environment suggests that this is the regime where collective fluctuations dominate. Rearrangements of many molecules appearing in density and polarization fluctuations destroy correlations for all of the order parameters after ≈200 fs.

Analyzing the interplay between local and collective electric fields sheds light on the types of molecular and cooperative motions that dephase the OH vibration. Specifically, Figure 9

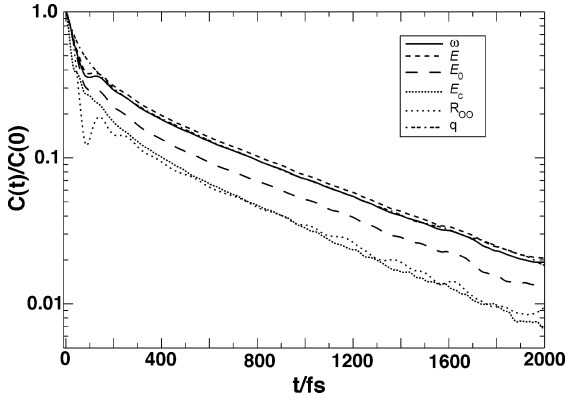

Figure 8. Semilog plot of the normalized time correlation functions for the order parameters studied in the text. The time constant of the exponential decay after ≈200 fs for qualitatively different order parameters is ≈600 fs. The long time decay of $C_{\omega\omega}(t)$ characterizes electric field fluctuations on longer length scales than the distance between molecules in the first solvation shell.

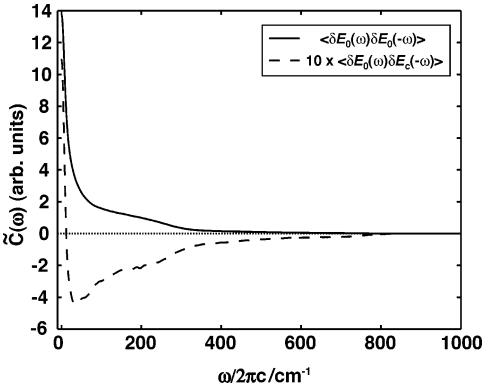

Figure 9. Fourier transform of the cross-correlation function (dashed line) between the local and collective electric field fluctuations revealing the phase relationship between these variables as a function of frequency. When HOD and its proximal hydrogen bonding partner approach each other and the local field strength increases, the medium polarizes in the opposite direction to minimize the electrostatic energy. The low-frequency peak, however, is in-phase with the local electric field fluctuations. Because this part of the spectral density corresponds to the exponential decay of the electric field fluctuations, the change in sign from negative to positive indicates that the long time exponential decay of correlations in Figure 8 is cooperative. The dotted black line is the baseline, included for contrast.

compares the Fourier transform of the correlation function $\tilde{C}(\omega) = \int_{-\infty}^{\infty} \mathrm{d}t\, C(t) \exp(\mathrm{i}\omega t)$ or the spectral density, for $\langle \delta E_0(t)\, \delta E_0(0)\rangle$, to that of the cross correlation function between the local and collective electric fields, $C_{\mathrm{cross}}(t) = \langle \delta E_c(t) \delta E_0(0)\rangle$. The integral over the spectral density of the cross correlation function is negative.

$$\int_0^{\infty} \mathrm{d}\omega\, \tilde{C}_{\mathrm{cross}}(\omega) = \pi C_{\mathrm{cross}}\,(t=0) \tag{21}$$

$$\rho_{E_c E_0} = \frac{C_{\mathrm{cross}}\,(t=0)}{\sigma_{E_c}\sigma_{E_0}} \tag{22}$$

$\rho_{E_c E_0}$ is the correlation coefficient between the local and collective electric fields. The integral in eq 21 averages over a dynamical quantity ($\tilde{C}_{\mathrm{cross}}(\omega)$) to return a static one ($\rho_{E_c E_0}$). Because $\rho_{E_c E_0}$ is negative, the local and collective electric fields are anticorrelated, but Figure 9 shows that only part of the spectral density is negative. The frequency dependence in Figure 9 reveals that the collective field counteracts changes that

increase the field strength between HOD and its hydrogen bonding partner when the frequency is larger than a few wavenumbers. The high-frequency molecular motions, librations, and hydrogen bond vibrations polarize against high-frequency changes in the local electric field. In other words, the local electric field is shielded from the more cooperative polarization fluctuations on short time scales. The zero frequency peak in $\tilde{C}_{\mathrm{cross}}(\omega)$ is positive. It corresponds to the long time exponential decay of $C_{\mathrm{cross}}(t)$, indicating that the motions that decorrelate E_c and E_0 at long times are in phase with each other. After ≈200 fs, the TCFs $\langle \delta E_0(t)\ \delta E_0(0)\rangle$ and $\langle \delta E_c(t)\ \delta E_c(0)\rangle$ decay exponentially and the local and collective fields fluctuate in concert with one another.

IV. Conclusions

We employed a simple adiabatic strategy combined with time-independent perturbation theory to compute vibrational frequencies of HOD in liquid D_2O with atomistic MD simulations. The strategy is accurate enough to reproduce many salient experimentally measured features of vibrational dephasing, is computationally efficient, and lends itself to a straightforward physical interpretation. The predictions of our model compare well with recent experimental data.[42] Joint probability distributions reveal statistical relationships among a set of physically motivated order parameters that classify the liquid environment and ω_{OH}. The correlation among ω_{OH} and the variables that describe local molecular geometries in the vicinity of the HOD molecule (q, $\cos(\alpha)$, R_{OO}) is a manifestation of the stronger underlying correlation between ω_{OH} and the electric field at the proton. The strong correlation between ω_{OH} and the electric field explains the weak connection between the frequency and the tetrahedrality of the first solvation shell, as well as the nearly azimuthal symmetry that Figure 2 displays about the OH axis on the red side of the line. As Figure 7 shows, adding the electric field contributions from molecules in the first solvation shell does little to improve upon the correlation between ω_{OH} and E_0 alone. The molecular features are apparent on short length scales.

Classical electrostatic forces are dominant (over, for example, dispersion forces) in determining the optical spectroscopy of polar liquids. Solvation dynamics experiments, for example, view the collective response of solvents in response to rapid changes in the charge distribution of a chromophore. Treating the solute's environment as a linearly responding polarizable medium often yields accurate predictions for the dynamics of solvation energy measured in experiments or computed in simulations.[50,51]

There is mounting evidence that vibrational dynamics in polar solvents are similarly governed by electrostatics. Rey and Hynes[34] found that the electrostatic forces dominated non-Coloumbic forces in their study of vibrational dynamics of the CN^- anion in water. Kwac and Cho[52] have computed vibrational frequencies for small peptides by solving the Schrödinger equation for the vibrational coordinate under the influence of the electrostatic potential from the peptide and solvent molecules. The physical picture we proposed in ref 32 and have described in detail in this paper is much simpler still: to a very good approximation, instantaneous vibrational frequency shifts are directly proportional to the liquid's electric field at a single point in space ($\mathbf{r}_{\mathrm{H}}$) projected onto a single direction ($\hat{\mathbf{r}}_{\mathrm{OH}}$). This connection is a powerful concept for interpreting and calculating spectral diffusion. Corcelli and Skinner,[53] for example, have recently exploited the strong correlation between the vibrational frequency and the electric field at the proton to devise a hybrid QM/MM method for computing vibrational frequencies.

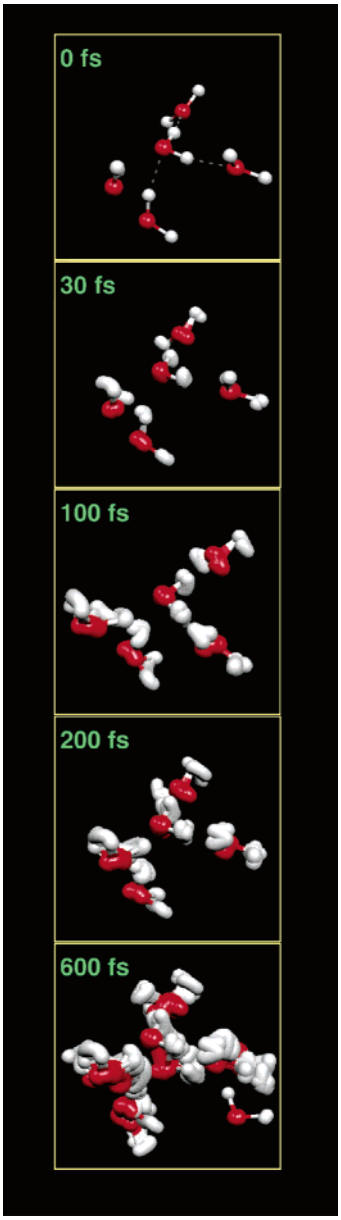

Figure 10. Evolution of time and length scales in water. Initially, the HOD molecule (center molecule) is hydrogen bonded to three partners. Between 30 and 100 fs, the molecular motions are small, localized fluctuations in the hydrogen bond network. After 200 fs, corresponding roughly to the correlation time of $C_{\omega\omega}(t)$, collective fluctuations destroy the structure of the first solvation shell. After 600 fs have passed, the molecules in the first solvation shell have little memory of their original positions and new molecular partners attempt entrance to the first solvation shell.

Previous experimental[20,45,54,55] and simulation[25,26,43] work has been driven by the empirical relationships built by Novak,[16] Badger,[14] and Rundle,[15] but the spectroscopy of the OH stretch of HOD in liquid D_2O is much richer than previously imagined. IR spectroscopy measures transient electric field fluctuations. At times prior to ≈200 fs, these dynamics characterize fluctuations on short length scales. Any information obtained from IR spectroscopies about local hydrogen bond interactions between HOD and its hydrogen bonding partner is unreliable after 200 fs because after this time the relaxation becomes collective. Figure 10 is a chronological "time-elapsed photograph" of how time and length scales evolve in water over several hundreds of femtoseconds and illustrates the changes in the liquid environment between 0 and 600 fs. In this figure, the spatial

positions of the atoms at an initial time blur over several frames but provide a picture of the molecular mechanism for vibrational dephasing. The initial events (30 fs) are molecular-sized librations. Because these motions project weakly onto the OH bond, they do not show up in $C_{\omega\omega}(t)$. Through the fast time decay and the beat (100−200 fs), the oxygen centers move appreciably. $C_{\omega\omega}(t)$ and R_{OO} reveal that these motions have an underdamped oscillation in the direction of R_{OO}. By 600 fs, approximately the time scale for the long time relaxation of $C_{\omega\omega}(t)$, there is little memory of the initial positions. In the last frame, a molecule attempts entrance into the first solvation shell.

At times (>200 fs) in $C_{\omega\omega}(t)$, there is a crossover to exponential relaxation that includes both molecular participants and collective density and polarization fluctuations. As Figure 9 shows, collective polarization fluctuations shield fast (≈200 fs) distortions of the local electric field. The characteristic shielding motions are the libration and hydrogen bond stretch of the D_2O molecules and are out-of-phase with the local electric field fluctuations. The long time decay, seen as a zero frequency resonance in the cross-correlation spectrum, is in-phase with the local electric field fluctuations. At long times, the relaxation originates from large scale cooperative reorganization and not from specific molecular motions such as hydrogen bond making and breaking, as some have suggested.[20,25,55,56] Previous pump−probe experiments have operated with a time resolution that is longer than the characteristic time of 200 fs[20,45,54,55] and, hence, probe the time scale of collective polarization fluctuations. Only recently have experimentalists performed measurements with sufficiently short time resolution to observe dynamics that occur on molecular length scales.[32,38,42,56,57]

Our picture of vibrational dephasing in water resonates with the Marcus theory of solvation dynamics, where, by analogy, the hydrogen bonding partner is an "inner shell" participant whose dynamics are buffeted by a polarizing solvent.[13] Our observations suggest that one may be able to understand the physical origin and qualitative features in vibrational dephasing experiments on hydrogen bonded systems with a highly simplified model. For HOD in liquid D_2O, the model should have only the HOD molecule and the hydrogen bonding partner as the essential molecular features. A linearly polarizable dielectric should be a good representation of the rest of the molecules. This picture may prove useful when one is interested in a reduced description for the spectroscopy of complex systems where fully atomistic simulations are computationally costly. Such systems might include large proteins with side chains and backbone atoms hydrogen bonded to the aqueous solution.

Acknowledgment. We thank the U.S. Department of Energy for support under grant DE-FG02-99ER14988. J.D.E. thanks David Reichman and Troy Van Voorhis for thoughtful discussions.

Appendix: Expansions in Internal Coordinates

A practical problem emerges when one computes the derivatives of the intermolecular potential in internal coordinates. Internal coordinates are functions of bond stretches and angles, for example. However, the intermolecular potential is a function of atomic Cartesian coordinates. More generically, internal coordinates are generalized coordinates that exclude overall translation and rotation of the molecule. Particular subtleties arise when one applies the chain rule of partial differentiation.

We illustrate the method employed to expand the hydride stretch coordinate to second order but emphasize that the method is simple and general. Direct expansions are sometimes not applied even to simple systems.[26,52] Instead, one finds the expansion numerically by evaluating the potential energy at several small displacements of the internal coordinate, gaining a more exact representation of H_{sb} at the expense of computational efficiency. More importantly, it is much easier to analyze a mathematical expression to determine which terms provide the largest perturbations than it is to backtrack through numerical computations. As long as the coupling between the vibration and the environment is a smoothly varying function, a low-order Taylor series approximation is sufficiently accurate. Direct expansion scales as $O(M-1)(\mathcal{N}^2)$, where M is the desired expansion order and $\mathcal{N}$ is the number of atoms in the system. It can be applied to systems with many atomic degrees of freedom that define an internal vibrational coordinate, including, but not limited to, small peptides and proteins in solution.

Begin with the derivative of the potential in internal coordinates. The potential is a function of atomic Cartesian coordinates, $V = V(\mathbf{r}_1, ..., \mathbf{r}_N)$. N is the number of atoms in the molecule. Allow k to be the number of equations of constraint that, for example, keep the center of mass of the chosen coordinate fixed. Because the equations of constraint are holonomic, the transformation equations between the atomic coordinates and generalized (internal) coordinates are

$$\begin{aligned}\mathbf{r}_1(t) &= \mathbf{r}_1(Q_1, ..., Q_{3N-k};t)\\ &\vdots\\ \mathbf{r}_N(t) &= \mathbf{r}_N(Q_1, ..., Q_{3N-k};t).\end{aligned} \tag{23}$$

We assume that these equations, along with the k equations of constraint, are invertible (the determinant of the Jacobian for the transformation in eq 23 is not singular). We are interested in the derivative of the potential with respect to some internal coordinate, Q_j. It is convenient to express the derivative operator by using the chain rule for partial derivatives.

$$\frac{\partial}{\partial Q_j} = \sum_{i=1}^{N} \frac{\partial \mathbf{r}_i}{\partial Q_j} \cdot \nabla_i \tag{24}$$

Applying the operator in eq 24 to the intermolecular potential provides an expansion in the set of Q_j to any order. If there is more than one generalized coordinate, H_{sb} is a multidimensional function whose expansion is facilitated by defining the operator,

$$D \equiv \sum_{i=1}^{3N-k} Q_i \frac{\partial}{\partial Q_i} \tag{25}$$

where it is understood that the partial derivatives act only to the right of D and by writing

$$H_{sb}(Q_1, ..., Q_{3N-k}) \approx \sum_{j=1}^{M} D^j \frac{H_{sb}(Q_1, ..., Q_{3N-k})}{j!} \tag{26}$$

where M is the desired order of the expansion and D^j is the operator in eq 25 raised to the jth power; upon expansion, all of the Q_j in the derivatives are evaluated at their equilibrium values in eq 26.

We demonstrate this technique by solving for the hydride stretch and give expressions for F and G used in the computation. Recall that we wrote the system-bath Hamiltonian that couples the vibrations to the environment as $H_{sb} = FQ + GQ^2$, where Q and Q^2 are both operators in the system eigenstate basis. For a stretch, the constraint is that the center of mass of the vibration remains fixed. The constraint is

$$\boldsymbol{R}_{\mathrm{com}} = \frac{\mathbf{r}_{\mathrm{H}} m_{\mathrm{H}} + \mathbf{r}_{\mathrm{O}} m_{\mathrm{O}}}{m_{\mathrm{O}} + m_{\mathrm{H}}} \tag{27}$$

We use the constraint equation explicitly by shifting to the center of mass frame and by writing the atomic positions relative to the center of mass

$$\mathbf{r}'_{\mathrm{H}} = -\frac{m_{\mathrm{O}}}{m_{\mathrm{O}} + m_{\mathrm{H}}}\mathbf{r} \tag{28}$$

$$\mathbf{r}'_{\mathrm{O}} = \frac{m_{\mathrm{H}}}{m_{\mathrm{O}} + m_{\mathrm{H}}}\mathbf{r} \tag{29}$$

where $\mathbf{r} = \mathbf{r}_{\mathrm{O}} - \mathbf{r}_{\mathrm{H}}$. With these substitutions, it is easy to express the derivatives in eq 24. The result is

$$\frac{\partial}{\partial Q} = \mu \hat{\mathbf{r}}_{\mathrm{OH}} \cdot \left(\frac{\nabla_{\mathrm{O}}}{m_{\mathrm{O}}} - \frac{\nabla_{\mathrm{H}}}{m_{\mathrm{H}}} \right) \tag{30}$$

where μ is the reduced mass and $\hat{\mathbf{r}}_{\mathrm{HO}}$ is the unit vector pointing from the oxygen to the hydrogen. To generate the first term in the expansion, F, we apply the derivative operator to the potential.

$$F = -\mu \hat{\mathbf{r}}_{\mathrm{OH}} \cdot \left(\frac{\mathbf{F}_{\mathrm{O}}}{m_{\mathrm{O}}} - \frac{\mathbf{F}_{\mathrm{H}}}{m_{\mathrm{H}}} \right) \tag{31}$$

where $\mathbf{F}_{\mathrm{H}}$ is the force on the hydrogen (oxygen). Evaluating this term with the Velocity−Verlet algorithm is free because the atomic forces are available at each time step. The expression for F is the same one that Rey and Hynes[34] used in their study of the vibrations of the CN^- anion in water. Evaluation of the second derivative, G, costs only $O(\mathcal{N}^2)$, whereas evaluation of H_{sb} for several values of Q costs $O(\mathcal{N}^2)$ at each step. We write

$$G = \frac{1}{2}\frac{\partial^2 V}{\partial Q^2} = \frac{\mu^2 \hat{\mathbf{r}}_{\mathrm{HO}} \hat{\mathbf{r}}_{\mathrm{HO}}}{2} : \left(\frac{\nabla_{\mathrm{O}} \nabla_{\mathrm{O}} V}{{m_{\mathrm{O}}}^2} - \frac{2 \nabla_{\mathrm{H}} \nabla_{\mathrm{O}} V}{m_{\mathrm{O}} m_{\mathrm{H}}} + \frac{\nabla_{\mathrm{H}} \nabla_{\mathrm{H}} V}{{m_{\mathrm{H}}}^2} \right) \tag{32}$$

where the : operator is the tensor contraction between the dyads on either side of the operator. Ewald summation of V partitions the sum over the molecules and their periodic images by a pairwise sum and a sum in reciprocal wavevector space, $V = V_{\mathrm{pair}} + V_{\mathbf{k}}$.

$$V = \frac{1}{2}\sum_{i=1}^{\mathcal{N}} \sum_{j=1, j\neq i}^{\mathcal{N}} \phi(|\mathbf{r}_i - \mathbf{r}_j|) + \sum_{\mathbf{k}} A(\mathbf{k}) |S(\mathbf{k})|^2 \tag{33}$$

In the above, $S(\mathbf{k}) = \sum_l z_l \, \mathrm{e}^{i\mathbf{k}\cdot\mathbf{r}_l}$ is the ionic structure factor, z_l is the charge of atom l, $A(k)$ is an amplitude, and $\phi(|\mathbf{r}_i - \mathbf{r}_j|)$ is the pair potential energy between atoms i and j. The double gradient operator on V contains three types of terms.

$$\nabla_\alpha \nabla_\beta V_{\mathrm{pair}} = -\left(\phi''(\mathbf{r}_{\alpha\beta}) \hat{\mathbf{r}}_{\alpha\beta} \hat{\mathbf{r}}_{\alpha\beta} + \frac{\phi'(\mathbf{r}_{\alpha\beta})}{r_{\alpha\beta}} (\mathbf{1} - \hat{\mathbf{r}}_{\alpha\beta} \hat{\mathbf{r}}_{\alpha\beta}) \right) \qquad (\alpha \neq \beta) \tag{34}$$

$$\nabla_\alpha \nabla_\alpha V_{\mathrm{pair}} = \sum_{\beta\neq\alpha} \left(\phi''(\mathbf{r}_{\alpha\beta}) \hat{\mathbf{r}}_{\alpha\beta} \hat{\mathbf{r}}_{\alpha\beta} + \frac{\phi'(\mathbf{r}_{\alpha\beta})}{r_{\alpha\beta}} (\mathbf{1} - \hat{\mathbf{r}}_{\alpha\beta} \hat{\mathbf{r}}_{\alpha\beta}) \right)$$

$$\nabla_\alpha \nabla_\beta V_{\mathbf{k}} = 2\sum_{\mathbf{k}} \mathbf{k}\mathbf{k} A(\mathbf{k}) z_\alpha \mathrm{Re}(\mathrm{e}^{-i\mathbf{k}\cdot\mathbf{r}_\alpha} [z_\beta \, \mathrm{e}^{i\mathbf{k}\cdot\mathbf{r}_\beta} - \delta_{\alpha\beta} S(\mathbf{k})]).$$

Substituting eq 34 into eq 32 yields the expression for G.

References and Notes

(1) Rahman, A.; Stillinger, F. H. *J. Am. Chem. Soc.* **1973**, *95*, 7943−7948.
(2) Stillinger, F. H. *Science* **1980**, *209* (4455), 451−457.
(3) Luzar, A.; Chandler, D. *Nature (London)* **1996**, *379*, 55−57.
(4) Stillinger, F. *Adv. Chem. Phys.* **1975**, *31*, 1−101.
(5) Teixeira, J.; Bellissent-Funel, M.-C.; Chen, S. H. *J. Phys.: Condens. Matter* **1990**, *2*, 105.
(6) Bosi, P.; Dupre, F.; Menzinger, F.; Sacchetti, F.; Spinelli, M. C. *Nuovo Cimento Lett.* **1978**, *21*, 436.
(7) Hasted, J.; Husain, S.; Frescura, F. A. M.; Birch, J. R. *Chem. Phys. Lett.* **1985**, *118*, 622.
(8) Sette, F.; Ruocco, G.; Krisch, M.; Bergmann, U.; Masciovecchio, C.; Mazzacurati, V.; Signorelli, G.; Verbeni, R. *Phys. Rev. Lett.* **1995**, *75* (5), 850−853.
(9) Fleming, G.; Cho, M. *Annu. Rev. Phys. Chem.* **1996**, *47*, 109−134.
(10) Fecko, C. J.; Eaves, J. D.; Tokmakoff, A. *J. Chem. Phys.* **2002**, *117* (3), 1139−1154.
(11) Lang, M. J.; Jordanides, X. J.; Song, X.; Fleming, G. R. *J. Chem. Phys.* **1999**, *110*, 5884−5892.
(12) Cho, M.; Fleming, G. R.; Saito, S.; Ohmine, I.; Stratt, R. M. *J. Chem. Phys.* **1994**, *100*, 6672−6683.
(13) Sumi, H.; Marcus, R. *J. Chem. Phys.* **1986**, *84* (9), 4894.
(14) Badger, R. M. *J. Chem. Phys.* **1940**, *8*, 288−289.
(15) Nakamoto, K.; Margoshes, M.; Rundle, R. *J. Am. Chem. Soc.* **1955**, *77*, 4670−4677.
(16) Novak, A. In *Structure and Bonding*; Dunitz, J. D., Hemmerich, P., Holm, R. H., Ibers, J. A., Jorgenson, C. K., Neilands, J. B., Reinen, D., Williams, R. J. P., Eds.; Springer-Verlag: New York, 1974; Vol. 18, pp 177−216.
(17) Volker, S. *Ann. Rev. Phys. Chem.* **1989**, *40*, 499−530.
(18) Jankowiak, R.; Hayes, J.; Small, G. *Chem. Rev.* **1993**, *93* (4), 1471−1502.
(19) Graener, H.; Seifert, G.; Laubereau, A. *Phys. Rev. Lett.* **1991**, *66*, 2092−2095.
(20) Woutersen, S.; Bakker, H. J. *Phys. Rev. Lett.* **1999**, *83*, 2077−2081.
(21) Gale, G. M.; Gallot, G.; Hache, F.; Lascoux, N.; Bratos, S.; Leicknam, J.-C. *Phys. Rev. Lett.* **1999**, 1068.
(22) Lawrence, C. P.; Skinner, J. L. *J. Chem. Phys.* **2002**, *117*, 5827−5838.
(23) Lawrence, C. P.; Skinner, J. L. *J. Chem. Phys.* **2002**, *117*, 8847−8854.
(24) Lawrence, C. P.; Skinner, J. L. *J. Chem. Phy.* **2003**, *118*, 264−272.
(25) Lawrence, C. P.; Skinner, J. L. *Chem. Phys. Lett.* **2003**, *369*, 472−477.
(26) Rey, R.; Moller, K. B.; Hynes, J. T. *J. Phys. Chem. A* **2002**, *106*, 11993−11996.
(27) Rey, R.; Moller, K. B.; Hynes, J. T. *Chem. Rev.* **2004**, *104*, 1915−1928.
(28) Berendsen, H.; Grigera, J.; Straatsma, T. *J. Phys. Chem.* **1987**, *91*, 6269−6271.
(29) Reimers, J. R.; Watts, R. *Mol. Phys.* **1984**, *52* (2), 357−381.
(30) Watson, I.; Henry, B.; Ross, I. *Spectrochim. Acta, Part A: Mol.Biomol. Spectrosc.* **1981**, *37* (10), 857−865.
(31) Oxtoby, D. W. *Adv. Chem. Phys.* **1979**, *40*, 1.
(32) Fecko, C.; Eaves, J.; Loparo, J.; Tokmakoff, A.; Geissler, P. *Science* **2003**, *301*, 1698−1702.
(33) Tully, J. *Faraday Discuss.* **1998**, *110*, 407−419.
(34) Rey, R.; Hynes, J. T. *J. Chem. Phys.* **1998**, *108*, 142.
(35) Fried, L. E.; Bernstein, N.; Mukamel, S. *Phys. Rev. Lett.* **1992**, *68* (12), 1842−1845.
(36) Egorov, S. A.; Rabani, E.; Berne, B. J. *J. Phys. Chem. B* **1999**, *103*, 10978−10991.
(37) Landau, L.; Teller, E. *Phys. Z. Sowjetunion* **1936**, *10*, 34.
(38) Loparo, J. J.; Fecko, C. J.; Eaves, J. D.; Roberts, S. T.; Tokmakoff, A. *Phys. Rev. B* **2004**, *70*, 180201(R).
(39) Allen, M.; Tildesley, D. *Computer Simulation of Liquids*; Oxford University Press: New York, 1989.
(40) Zwanzig, R. *Nonequilibrium statistical mechanics*; Oxford University Press: New York, 2001.
(41) Mukamel, S. *Principles of Nonlinear Optical Spectroscopy*; Oxford University Press: New York, 1998.
(42) Fecko, C.; Loparo, J.; Roberts, S. R.; Tokmakoff, A. *J. Chem. Phys.* **2005**, *122*, 054506-1−054506-18.
(43) Moller, K. B.; Rey, R.; Hynes, J. T. *J. Phys. Chem. A* **2004**, *108*, 1275−1289.
(44) Errington, J. R.; Debenedetti, P. G. *Nature* **2001**, *409*, 318−321.
(45) Laenen, R.; Rauscher, C.; Laubereau, A. *J. Phys. Chem. B* **1998**, *102*, 9304−9311.
(46) Laenen, R.; Rauscher, C.; Laubereau, A. *Phys. Rev. Lett.* **1998**, *80*, 2622−2625.
(47) Balucani, U.; Torcini, R. G. A.; Vallauri, R. *Phys. Rev. E* **1993**, *47* (3), 1677−1684.

(48) Balucani, U.; Ruocco, G.; Sampoli, M.; Torcini, A.; Vallauri, R. *Chem. Phys. Lett.* **1993**, *209* (4), 408−416.

(49) Teixeira, J.; Bellissent-Funel, M.-C.; Chen, S. H.; Dorner, B. *Phys. Rev. Lett.* **1985**, *54* (25), 2681−2683.

(50) Song, X.; Chandler, D. *J. Chem. Phys.* **1998**, *108*, 2594−2600.

(51) Song, X.; Chandler, D.; Marcus, R. *J. Phys. Chem.* **1996**, *100*, 11954−11959.

(52) Kwac, K.; Cho, M. *J. Chem. Phys.* **2003**, *119* (4), 2247−2255.

(53) Corcelli, S. A.; Lawrence, C. P.; Skinner, J. L. *J. Chem. Phys.* **2004**, *120*, 8107−8117.

(54) Kropman, M. F.; Nienhuys, H.-K.-W.; Woutersen, S.; Bakker, H. J. *J. Phys. Chem. A* **2001**, *105*, 4622−4626.

(55) Bratos, S.; Gale, G. M.; Gallot, G.; Hache, F.; Lascoux, N.; Leicknam, J. C. *Phys. Rev. E* **2000**, *61* (5), 5211−5217.

(56) Yeremenko, S.; Pshenichnikov, M. S.; Wiersma, D. A. *Chem. Phys. Lett.* **2003**, *369*, 107−113.

(57) Asbury, J. B.; Steinel, T.; Stromberg, C.; Corcelli, S. A.; Lawrence, C. P.; Skinner, J. L.; Fayer, M. D. *J. Phys. Chem. A* **2004**, *108*, 1107−1119.